Disaster Resilience Management of Civil Infrastructure Systems based on Reliability, Redundancy, and Recoverability

Junho Song
Professor, Dept. of Civil and Environmental Engineering, Seoul National University, Seoul, South Korea

ABSTRACT: As the complexity of civil infrastructure systems is ever-increasing amid various uncertainties, their resilience against natural and human-made disasters should be managed based on a holistic understanding of the systems' performance under hazards. To address this need, the author's research group recently proposed a system reliability-based framework characterizing disaster resilience by three criteria: reliability, redundancy, and recoverability. In particular, the reliability (β) and redundancy (π) indices were defined to quantify the system's component- and system-level abilities against initial disruption scenarios and their cascading effects, respectively. The pairs of the indices are visualized in a scatter plot termed "β-π diagram" to facilitate resilience-informed decision-making. After briefly reviewing the framework, this paper introduces its recent applications to a real-world cable-stayed bridge under tank truck fire hazards and complex infrastructure networks under seismic hazards, demonstrating its benefits and potential in the disaster resilience management of complex civil infrastructure systems. The paper also introduces the ongoing development of a resilience-based decision optimization algorithm to automate resilience-informed decision-making processes as a core technology supporting risk intelligence of civil infrastructure systems.

1. INTRODUCTION

The traditional *stability* viewpoint in ecology pursued minimum fluctuations and equilibrium in a predictable world. As an alternative, the *resilience* viewpoint (Hollings, 1973) was proposed to understand and promote the system's ability to absorb and accommodate significant uncertainties and inevitable changes in the future. Since then, the concept has been studied in various engineering fields to achieve the holistic ability of a system to sustain external and internal disruptions without discontinuity of the original functionality or, if discontinued, to recover fully and rapidly (Zhou et al., 2010; Hosseini et al., 2016; ASME, 2009).

The disaster resilience of civil infrastructure systems has been investigated as a multi-aspect concept. For example, in earthquake engineering, resilience was defined in terms of four criteria: robustness, redundancy, resourcefulness, and rapidity (Bruneau et al., 2003). Probabilistic resilience indices were also developed to consider uncertainties in hazards and engineering systems (Hashimoto et al., 1982; Chang and Shinozuka, 2004). There have also been numerous efforts to understand disaster resilience using the "resilience triangle" (Tierney and Bruneau, 2007), which describes the loss of system functionality and recovery patterns in the performance restoration curves.

Despite significant advancements in theories, further research is still needed for the effective management of disaster resilience of civil infrastructure systems. First, the definition of the performance measure in the restoration curves is often subjective and lacks the multi-aspect concept. Second, because the functionality and socioeconomic utility depend on the system-level performance, disaster resilience analyses demand a *systems* perspective based on a holistic understanding of the relationship between component reliability and system redundancy. Third, the ultimate goal of disaster resilience evaluations is to make better or optimal decisions. Therefore, it is essential to build an analysis framework that streamlines disaster resilience management.

To address these research needs, the author's research group recently proposed a system reliability-based disaster resilience analysis (S-DRA) framework (Lim et al., 2022a) that hinges on three criteria: reliability, redundancy, and recoverability. The framework also introduces indices for the reliability and redundancy criteria, which reveal probabilistic interrelationships between the system and its components. A graphical tool termed "β-π diagram" was also proposed to support decision-making processes by the resilience analysis results.

This paper briefly reviews the framework (Section 2) and introduces its recent applications to a real-world cable-stayed structure under tank truck fire hazards (Section 3) and infrastructure networks under seismic hazards (Section 4). Ongoing research efforts to automate resilience-informed decision-making are also introduced (Section 5). The paper is concluded with a summary and remarks.

2. SYSTEM-RELIABILITY-BASED DISASTER RESILIENCE FRAMEWORK

The three criteria of the S-DRA framework (Lim et al., 2022a) are illustrated in Figure 1. The ball near the edge of a cliff, representing a civil infrastructure system of interest, could fall due to natural or human-made hazards, represented by the purple arrow. The red wall represents the *reliability* criterion, defined as the components' ability to avoid initial disruptions despite disastrous events. The blue wall symbolizes *redundancy*, defined as the system's capability of preventing cascading system-level failure given the initial disruption. The yellow arrows describe *recoverability*, defined as the ability of the community and engineers to restore the system's functionality to its original state. Detailed definitions of the criteria depend on the resilience analysis scale, such as individual structure, infrastructure network, and urban community, as summarized in the "3x3 resilience matrix" (Lim et al., 2022a).

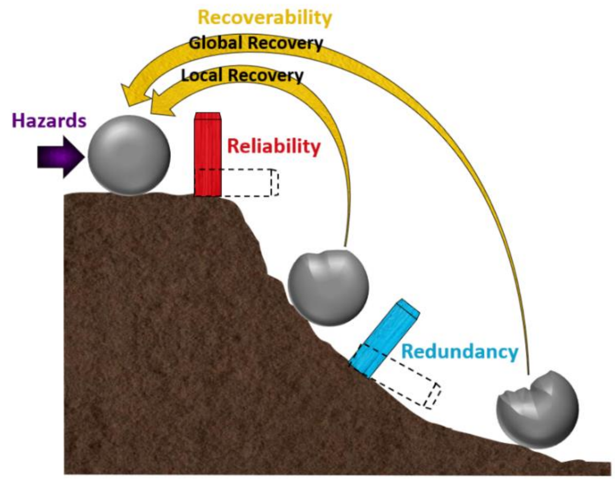

Figure 1: Three criteria of system reliability-based disaster resilience analysis framework (modified from Lim et al. (2022a))

To relate the multi-aspect resilience concept with component and system reliability analyses, the reliability (β) and redundancy (π) indices are respectively defined as

$$\beta_{i,j} = -\Phi^{-1}\left(P\left(F_i \middle| H_j\right)\right) \tag{1a}$$

$$\pi_{i,j} = -\Phi^{-1}\left(P\left(F_{sys} \middle| F_i, H_j\right)\right) \tag{1b}$$

where $\Phi^{-1}(\cdot)$ denotes the inverse cumulative distribution function (CDF) of the standard normal distribution, F_i is the i^{th} initial disruption scenario, H_j is the j^{th} hazard, and F_{sys} is the system failure event. Appropriate methods for component and system reliability analysis should be selected to calculate β and π based on the characteristics of the probabilistic hazard model and the limit-state functions describing initial disruptions and system failure events.

For the j^{th} hazard with the occurrence rate λ_{H_j}, the indices in Eq. (1) can be used to determine the annual system failure probability induced by the i^{th} disruption scenario as

$$\begin{aligned} P\left(F_{sys,i,j}\right) &= P\left(F_{sys,i,j} \middle| H_j\right)\lambda_{H_j} \\ &= P\left(F_{sys} \middle| F_i, H_j\right)P\left(F_i \middle| H_j\right)\lambda_{H_j} \\ &= \Phi\left(-\pi_{i,j}\right)\Phi\left(-\beta_{i,j}\right)\lambda_{H_j} \end{aligned} \tag{2}$$

The following resilience constraint can be introduced to make sure the annual system failure probability is socially acceptable:

$$\Phi(-\pi_{i,j})\Phi(-\beta_{i,j}) < \frac{P_{dm}}{\lambda_{H_j}} \tag{3}$$

where P_{dm} denotes *de minimis risk* (Pate-Cornell, 1994), i.e., the level of risk for which society imposes no regulations (Ellingwood, 2006).

Lim et al. (2022a) proposed to show the reliability and redundancy indices, calculated for initial disruption scenarios of interest, in a scatter plot termed reliability-redundancy (β-π) diagram, as shown in Figure 2. The black solid curve represents the contour of zero resilience margin, i.e., $\Phi(-\pi_{i,j})\Phi(-\beta_{i,j}) = P_{dm}/\lambda_{h_j}$. Therefore, the diagram quickly identifies initial disruption scenarios that violate the resilience constraint in Eq. (3). For example, the system-level risk induced by the initial disruption scenarios #13, #15, and #17 are not socially acceptable due to low reliability or redundancy. For the constraint-violating initial disruption scenarios, decision-makers must identify optimal decisions and actions such as hazard mitigations, changes in design or operation, and retrofits to ensure proper disaster resilience.

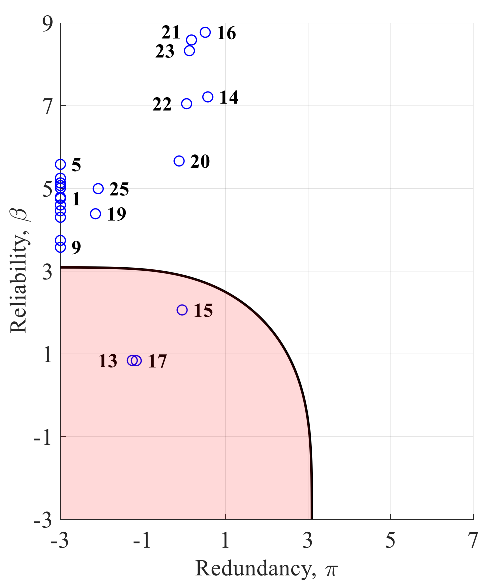

Figure 2: β-π diagram of a truss bridge with the resilience constraint (modified from Lim et al. (2022a))

3. β-π ANALYSIS OF CABLE-STAYED BRIDGE UNDER FIRE TRUCK HAZARDS

The applicability of the S-DRA framework to real-world complex structures was demonstrated through its application to the Seohae Grand Bridge, located on the west coast of South Korea (Lim et al., 2022b).

3.1. Probabilistic model of tank truck fire hazard

Because of its location near major industrial complexes, the Seohae Grand Bridge is exposed to the significant risk of structural failures caused by excessive heat from tank truck fires on the deck (Figure 3).

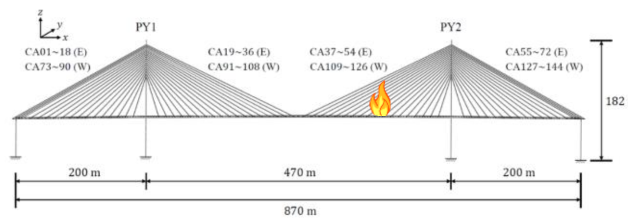

Figure 3: The Seohae Grand Bridge subjected to tank truck fire hazards

To develop a probabilistic model of tank truck fire hazards, Lim et al. (2022b) first identified three basic random variables, $\mathbf{X} = [A, X, \sigma\varepsilon]^{\mathrm{T}}$ where A is the area of pool fire (uniform), X denotes the longitudinal location of the fire on the third lane of the bridge (uniform), and $\sigma\varepsilon$ is the residual (normal) in the regression model of the effective emissive power of the flame (E) on the equivalent diameter $D = \sqrt{4A/\pi}$, i.e., $\ln E = 4.0228 - 0.0822 \ln D + \sigma\varepsilon$ (Shokri and Beyler, 1989).

The uncertainties in $\mathbf{X}$ are propagated through the heat radiation mechanism illustrated in Figure 4 to the radiative heat flux at cables. In the figure, $\dot{Q}$ is the heat release rate (100MW used in the example), $H(= 0.235\dot{Q}^{2.5} - 1.02D)$ is the height of the pool fire flame, and F_{12} is the configuration factor, defined as the ratio of the heat flux at a target to that of source locations. The final heat flux is computed as $\dot{q}'' = E \times F_{12}$.

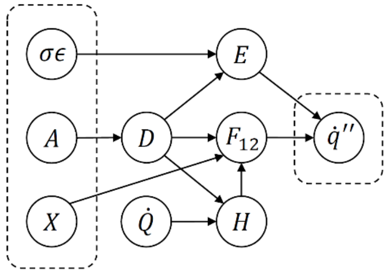

Figure 4: Graph model describing the uncertainty propagation from basic random variables to the radiative heat flux

3.2. Procedure for β-π analysis of the Seohae Grand Bridge

The limit-state functions for the indices β and π in Eq. (1) regarding the i^{th} initial disruption scenario, i.e., the i^{th} cable, are defined as follows:

$$g_i^{\beta}(\mathbf{u}) = \sigma_i^{y}(\mathbf{u}) - \sigma_i^{\beta}(\mathbf{u}) \tag{4a}$$

$$g_i^{\pi}(\mathbf{u}) = \min\begin{pmatrix} \sigma_{i-1}^{y}(\mathbf{u}) - \sigma_{i-1}^{\pi,i}(\mathbf{u}) \\ \sigma_{i+1}^{y}(\mathbf{u}) - \sigma_{i+1}^{\pi,i}(\mathbf{u}) \end{pmatrix} \tag{4b}$$

where $\mathbf{u}(=[u_A, u_X, u_{\sigma\epsilon}]^{\text{T}})$ denotes a realization of the basic random variables $\mathbf{X}$, transformed to standard normal random variables, $\sigma_i^{y}(\mathbf{u})$ is the yield strength of the i^{th} cable considering the strength degradation given $\mathbf{u}$, $\sigma_i^{\beta}(\mathbf{u})$ denotes the stress applied to the i^{th} cable, obtained from structural analysis, and $\sigma_{i-1}^{\pi,i}(\mathbf{u})$ and $\sigma_{i+1}^{\pi,i}(\mathbf{u})$ are respectively the stresses applied to the $(i-1)^{\text{th}}$ and $(i+1)^{\text{th}}$ cables after the initial disruption at the i^{th} cable. The 'min' operator is utilized because the system failure is defined as the union of the two adjacent cables' failures.

During reliability analyses, the stresses in Eq. (4) are simulated as follows: 20 temperature nodes are added to each cable (1~20 m above the deck) of the ABAQUS® model of the Seohae Grand Bridge (Lee et al., 2022). The temperature at each node is determined by pre-calculated solutions to a transient conduction equation. The degradation of Young's modulus and thermal expansion are incorporated into the finite element model based on the determined temperature. Lim et al. (2022b) developed Python codes that can execute ABAQUS® simulations within the reliability analysis codes in MATLAB® environment to obtain the stresses in the cables.

For efficient reliability analyses, the Active learning reliability method combining Kriging and Monte Carlo Simulation (AK-MCS; Echard et al., 2011) is used. In calculating the redundancy index, causal effects from the i^{th} scenario, F_i, such as load re-distributions, progressive failures, and dynamic effects are considered. In addition, the sampling for the redundancy index calculations is performed in the domain of F_i.

3.3. Results

Figure 5 shows the indices computed by the reliability analyses (on top of the corresponding cable locations). The reliability indices vary depending on the load distributions over the cables, whereas the redundancy indices are affected by the angles of the cable (which determines the affected length) and the number of adjacent cables (i.e., one or two).

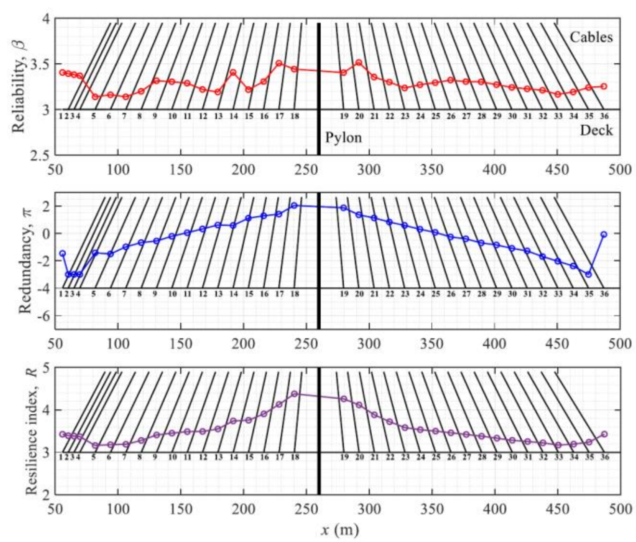

Figure 5: Indices for reliability, redundancy, and resilience ($R_{i,j} = -\Phi^{-1}(\Phi(-\pi_{i,j})\Phi(-\beta_{i,j}))$) *(Lim et al. (2022b))*

Next, the reliability and redundancy indices of each initial disruption scenario (i.e., cable failure) are shown in the β-π diagram (Figure 6) for $P_{dm} = 10^{-7}/\text{year}$. The annual occurrence rate of tank truck fires, $\lambda_H^{calculated}$ is estimated as

1.124×10^{-4}/year based on the statistics of the fire events and the annual mileage of tank trucks passing through the bridge. The solid line in the figure represents the contour of zero resilience margin for $\lambda_H^{calculated}$. All markers are found to satisfy the resilience constraint. However, when the annual occurrence rate is $\lambda_H^{assumed} = 1.686 \times 10^{-4}$/year based on the assumption of a 50% increase in the annual truck traffic, seven cables are violating the resilience constraint. Based on this result, resilience-informed decisions need to be made for these cables, e.g., reinforcing the cables, installing fire protection walls beside the cables, equipping the bridge with fire extinguishing facilities, and controlling the daily traffic of tank trucks on the bridge.

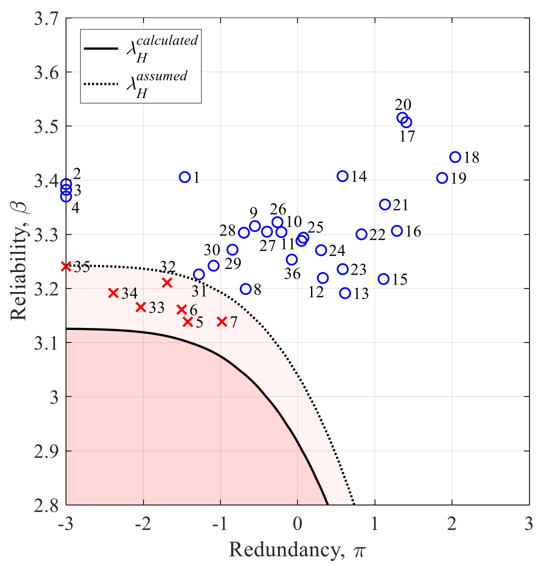

Figure 6: β-π diagram of the Seohae Grand Bridge under tank truck fire hazards (modified from Lim et al. (2022b)

4. β-π ANALYSIS OF INFRASTRUCTURE NETWORKS UNDER SEISMIC HAZARDS

The applicability of the S-DRA framework to general infrastructure networks was recently demonstrated by Kwon and Song (2023). Causality-based importance measures of network components were also proposed based on the β-π analysis framework.

4.1. S-DRA of bridge network under seismic hazards

The bridge transportation network in Sioux Falls, USA, features highways and interior arterial roads. Figure 7 shows a simplified model of the network consisting of 19 bridges, of which structural types are multi-span simply-supported concrete girders located on the highways and single-span concrete girders in downtown areas (Nielson and DesRoches, 2007). A virtual city with the same network topology is assumed to be affected by a 7.5-magnitude earthquake occurring at the coordinate (–4,6) in the figure. The network-level performance objective is to maintain post-disaster connectivity between the two sets of source and terminal nodes.

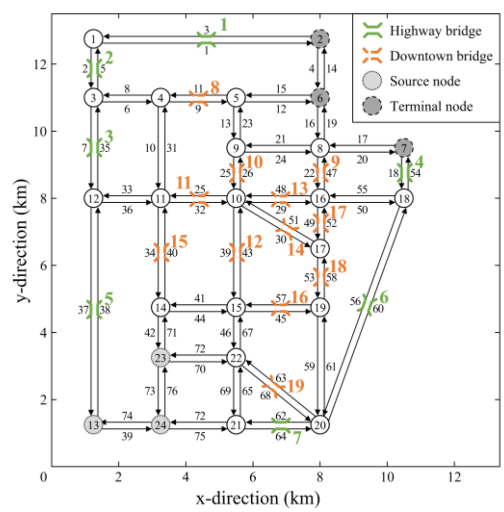

Figure 7: Virtual network model consisting of two types of 19 bridges having the same network topology of Sioux Falls, USA

The ground motion prediction equation (GMPE) for the logarithm of the peak ground acceleration (PGA) at the bridge e by the jth earthquake H_j can be described as

$$\ln D_{je} = F(M_j, R_{je}) + \eta_j + \varepsilon_{je} \quad (5)$$

where $F(\cdot)$ is the function predicting the mean-log PGA, M_j is the j^{th}earthquake magnitude, R_{je} is the distance between the epicenter and the bridge e, and η_j and ε_{je} are inter- and intra-event residuals, respectively. If σ_η^2 and σ_ε^2 represent the variances of the uncertainties, the total variance of $\ln D_{je}$, σ_T^2 is $\sigma_\eta^2 + \sigma_\varepsilon^2$.

Following HAZUS-MH (FEMA), the capacity of structure e for damage state DS, C_e^{DS} is assumed to follow a lognormal distribution with parameters $\ln\alpha_e^{DS}$ and β_e^{DS}, i.e., $C_e^{DS} \sim LN(\ln\alpha_e^{DS}, (\beta_e^{DS})^2)$. The structure e under H_j fails as D_{je} exceeds C_e^{DS} with the probability

$$\begin{aligned} P(E_e|H_j) &= P(\ln C_e^{DS} \leq \ln D_{je}) \\ &= P\left(Z_{je} \leq -\frac{\ln\alpha_e^{DS} - F(M_j, R_{je})}{\sqrt{(\beta_e^{DS})^2 + \sigma_T^2}}\right) \\ &= \Phi\left(-\frac{\ln\alpha_e^{DS} - F(M_j, R_{je})}{\sqrt{(\beta_e^{DS})^2 + \sigma_T^2}}\right) \end{aligned} \tag{6}$$

where Z_{je} is the standard normal random variable describing the reliability of structure e under H_j. The correlation coefficient between Z_{je_1} and Z_{je_2} of two structures e_1 and e_2 is derived as

$$\rho_{1,2}^j = \frac{\sigma_\eta^2 + \rho_{e_1e_2}(\Delta)\sigma_\varepsilon^2}{\sqrt{\left(\left(\beta_{e_1}^{DS}\right)^2 + \sigma_T^2\right)\left(\left(\beta_{e_2}^{DS}\right)^2 + \sigma_T^2\right)}} \tag{7}$$

where Δ denotes the distance between the two structures, and $\rho_{e_1e_2}(\Delta)$ is an underlying spatial correlation model, e.g., $\exp(-0.27\Delta^{0.4})$ (Lim et al., 2012).

Adopting the GMPE in Eq. (5) from Boore and Atkinson (2008) with $V_{S30} = 760\text{m/s}$, the reliability and redundancy indices for the i^{th} initial disruption scenario involving k component failures, F_i^k, can be computed using the component failure probabilities in Eq. (6) and the correlation coefficients in Eq. (7). The reliability index β_i^k requires calculating a k-variate normal CDF. The redundancy index π_i^k can be calculated based on the identified cut sets causing network-level performance loss (Kwon and Song, 2023).

Figure 8 shows the β-π diagram of the Sioux Falls bridge network. The filled markers represent the results that fully consider the correlations between bridge states, while hollow markers are obtained with correlation effects ignored. As the number of failed components (k) increases, its probability decreases (i.e., the reliability index increases), and the redundancy of the damaged system decreases (markers moving from the top left to the bottom right). It is also noted that both reliability and redundancy indices significantly overestimate the disaster resilience of the network when correlations are ignored.

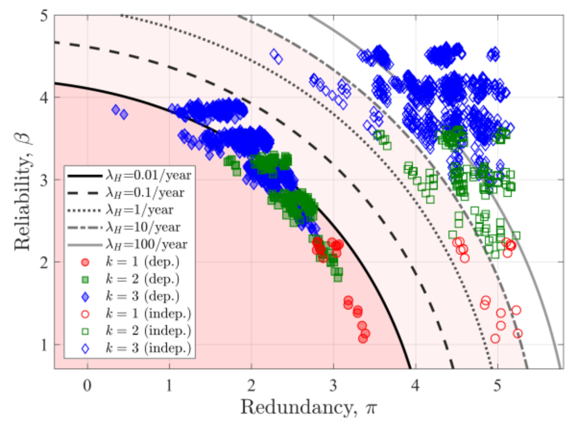

Figure 8: β-π diagram of Sioux Falls bridge network for dependent and independent component states

4.2. Causality-based importance measures beyond the β-π analysis

Kwon and Song (2023) proposed a β-π analysis-based method to quantify the relative importance of network components considering the causality effects of the initial disruptions. Figure 9 shows the causal diagram representing the network connectivity loss Y_{net} induced by external hazards S_j. U represents a set of factors affecting the component states X_e, $e = 1, \ldots, n$, considered an unobservable variable to acknowledge imperfect knowledge of the component states.

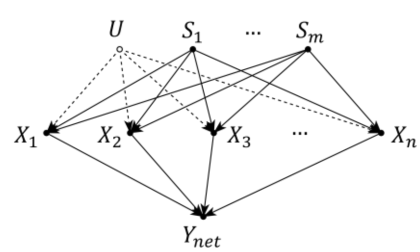

Figure 9: Causal diagram describing network-level connectivity loss by seismic hazards

From a causal viewpoint, it is crucial to exclude the spurious associations arising from common causes U and m sources in the causal diagram. *Do*-operator enables quantifying causal effects on the system reliability by enforcing the state of a particular component. For component e belonging to the index set of F_i^k, its causal contribution $C_{i,e}^k$ is quantified as

$$C_{i,e}^k = \sum_F r_e^k(F)P(F|H) \quad (8)$$

where $r_e^k(F)$ denotes the rate of change in system reliability caused by component state change by the *do*-operator (Kwon and Song, 2023). Based on the causal contribution in Eq. (8), the causality-based importance measure (CIM) and normalized CIM (NCIM) are respectively defined as

$$\mathrm{CIM}_e^k = \sum_{i:(\pi_i^k,\beta_i^k)\notin\mathcal{D}} \Phi(-\pi_i^k)\Phi(-\beta_i^k)C_{i,e}^k \quad (9a)$$

$$\mathrm{NCIM}_e^k = \mathrm{CIM}_e^k/\max_e(\mathrm{CIM}_e^k) \quad (9b)$$

where $\mathcal{D}$ is the domain in the β-π diagram, satisfying the resilience constraint in Eq. (3). Figure 10 shows NCIM^k of the Sioux Falls bridge network under scenarios with $k = 1, \dots, 3,$ for dependent and independent component states.

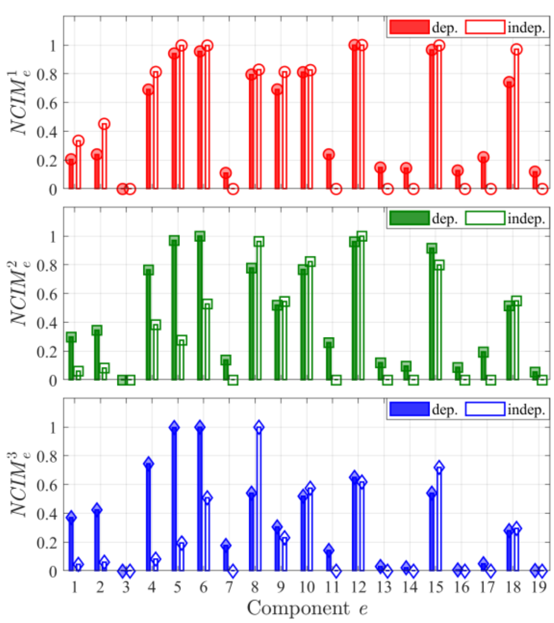

Figure 10: $NCIM^k$ of the Sioux Falls bridge network for dependent ($\lambda_H = 0.01/year$) and independent ($\lambda_H = 10/year$) component states

5. RELIABILITY-REDUNDANCY-RECOVERABILITY-BASED DECISION OPTIMIZATION

Reliability-Redundancy-Recoverability-based decision optimization (R3-DO) algorithm (Lim et al., 2023) was recently developed to support optimal decision-making based on the S-RDA framework.

5.1. Problem formulation

The R3-DO algorithm aims to achieve the minimum value of the cost function, indicating maximum recoverability while satisfying the disaster resilience constraint in Eq. (3) defined in terms of the reliability and redundancy indices for initial disruption scenarios of interest. Accordingly, the R3-DO algorithm is formulated as

$$\begin{aligned} &\min.\ f_{cost}(\boldsymbol{\theta}) \\ &\text{s.t.}\ \ \Phi(-\pi_i(\boldsymbol{\theta}))\Phi(-\beta_i(\boldsymbol{\theta})) < P_{dm}/\lambda_H \quad (10) \\ &\quad\ \ for\ i = 1, \dots, n_{sc} \end{aligned}$$

where $\boldsymbol{\theta}$ denotes the design parameter vector, typically including the mean values of random variables, $f_{cost}(\boldsymbol{\theta})$ indicates the total cost function, and n_{sc} is the number of disaster resilience constraints, i.e., the number of initial disruption scenarios of interest.

5.2. Cost functions of R3-DO

R3-DO pursues maximum recoverability by including not only the initial cost but also the recovery cost in the definition of the total cost function $f_{cost}(\boldsymbol{\theta})$. For a holistic coverage of the recoverability, the recovery actions are divided into (1) local recovery and (2) global recovery, i.e., the two yellow arrows in Figure 1. The local recovery indicates the recovery right after the initial disruption scenario. On the other hand, global recovery denotes the recovery performed after the system failure. Therefore, the total cost function of R3-DO, $f_{cost}(\boldsymbol{\theta})$ is defined as the sum of the initial, local-recovery, and global-recovery costs as

$$f_{cost}(\boldsymbol{\theta}) = IC(\boldsymbol{\theta}) + ELRC(\boldsymbol{\theta}) + EGRC(\boldsymbol{\theta}) \tag{11}$$

where $IC(\boldsymbol{\theta})$ denotes the initial cost, $ELRC(\boldsymbol{\theta})$ is the expected cost for the local recovery, and $EGRC(\boldsymbol{\theta})$ is the expected cost for the global recovery.

For the detailed formulation, the i^{th} element of design parameter vector $\boldsymbol{\theta}$, θ_i, is assumed to be the design parameter corresponding to the i^{th} initial disruption scenario. Then, each of the cost functions in Eq. (11) is defined as

$$IC(\boldsymbol{\theta}) = \sum_{i=1}^{n_{sc}} \theta_i \tag{12a}$$

$$\begin{aligned} ELRC(\boldsymbol{\theta}) &= \sum_{i=1}^{n_{sc}} ELRC_i(\boldsymbol{\theta}) \\ &= \sum_{i=1}^{n_{sc}} LRC_i(\boldsymbol{\theta}) P\left(F_i \middle| H_j\right) \end{aligned} \tag{12b}$$

$$\begin{aligned} &EGRC(\boldsymbol{\theta}) \\ &\quad = GRC(\boldsymbol{\theta}) \sum_{i=1}^{n_{sc}} P\left(F_{sys,i,j} \middle| H_j\right) \end{aligned} \tag{12c}$$

where $ELRC_i(\theta_i)$ indicates the expected cost for the local recovery caused by the i^{th} initial disruption scenario; $LRC_i(\theta_i)$ denotes the cost of the local recovery caused by the i^{th} initial disruption scenario; and $GRC(\boldsymbol{\theta})$ is the cost of the global recovery induced by the system failure F_{sys}. The recovery costs $LRC_i(\theta_i)$ and $GRC(\boldsymbol{\theta})$ are multiplied by the corresponding failure probabilities to evaluate the expected costs. Alternatively, the probabilities in Eqs. (12b) and (12c) can be described using the β and π indices according to Eqs. (1a) and (1b).

5.3. Constraints of R3-DO

The disaster resilience constraint in Eq. (3) is set as the constraint for R3-DO. This implies that the optimal solution of R3-DO should have the socially acceptable risk of system failure, which can be accomplished by securing a certain level of reliability and redundancy. From the viewpoint of the β-π diagram, R3-DO performs the optimization while pushing the β-π points to the outside of the contour of zero resilience margin so that the optimization result should be located in the domain $\mathcal{D}$ satisfying the resilience constraint in Eq. (3). For example, the decision behind the diagram in Figure 2 is not accepted by R3-DO because of the initial scenarios #13, #15, and #17.

5.4. Numerical example

The example truss bridge in Figure 11 is investigated to demonstrate the applicability and effectiveness of R3-DO. The truss bridge has 25 members whose yield stresses are 276 Mpa. The truss example is composed of 30 basic random variables: a cross-sectional area of 25 members, $A_i, i = 1, \ldots 25$, and external loads, $P_i, i = 1, \ldots 5$. The i^{th} cross-sectional area A_i is modeled as a normal random variable whose mean value is considered the design parameter θ_i. The coefficient of variation (c.o.v.) of A_i is assumed to be 0.05. The external loads, P_i, $i = 1, \ldots 5$, respectively follow normal distributions with means of 120 kN, 140 kN, 140 kN, 120 kN, and 120 kN. The c.o.v. is assumed to be 0.3 for each P_i. The hazard occurrence rate λ_j is assumed to be 10^{-4}/year. The initial point of the design parameter vector is set as $\boldsymbol{\theta}^{(0)} = $ [32, 32, 32, 32, 32, 32, 24, 24, 24, 24, 24, 24, 5, 5, 5, 5, 5, 7, 7, 7, 7, 7, 7, 7, 7] $\times 10^{-4}$ m^3.

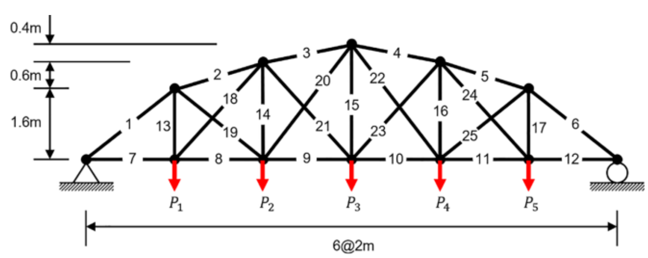

Figure 11: Configuration of truss system consisting of 25 members (Lim et al., 2023)

Twenty-five single-member failures are assumed as initial disruption scenarios for the β-π analysis. The system failure event for the redundancy index calculations is defined as (1) a cascading failure among remaining cables or (2) static instability caused by an initial disruption scenario. The local and global recovery cost functions are defined as $LRC_i(\theta_i) = a_i\theta_i$ and $GRC(\boldsymbol{\theta}) = \boldsymbol{b}^{\mathrm{T}}\boldsymbol{\theta}$, where a_i and $\boldsymbol{b}$ denote the normalized local recovery cost for the i^{th} initial disruption scenario and the normalized global recovery cost, respectively. The First-Order Reliability Method (FORM; see Der Kiureghian (2022)) and Sequential Compounding Method (Kang and Song, 2010) are employed to efficiently perform component- and system-reliability analyses and corresponding sensitivity calculations.

The convergence histories of the cost function and design parameters by R3-DO in Figure 12 demonstrate that R3-DO successfully achieves optimal design parameters minimizing the total cost function after around 140 iterations. The optimal design parameters are identified as $\boldsymbol{\theta}^{\text{optimal}} = [29, 28, 27, 27, 27, 28, 23, 23, 25, 25, 22, 22, 9, 3, 9, 3, 9, 1, 8, 6, 1, 4, 1, 1, 7] \times 10^{-4}\ \mathrm{m}^3$. Figure 13 visualizes the R3-DO procedure in the β-π diagram by the indices at iteration steps #1, #75, and #140. The β-π diagram at iteration step #140 shows that R3-DO succeeded in identifying optimal design parameters that minimize the cost function while placing all β-π points in the zone satisfying the resilience constraint.

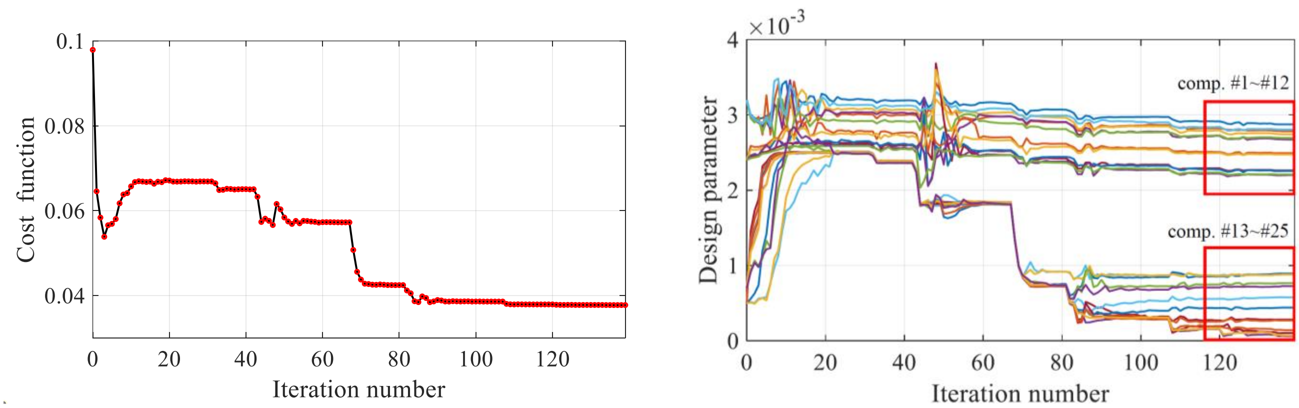

Figure 12: Convergence histories of the cost function (left) and design parameters (right) for R3-DO of the 25-member-truss system

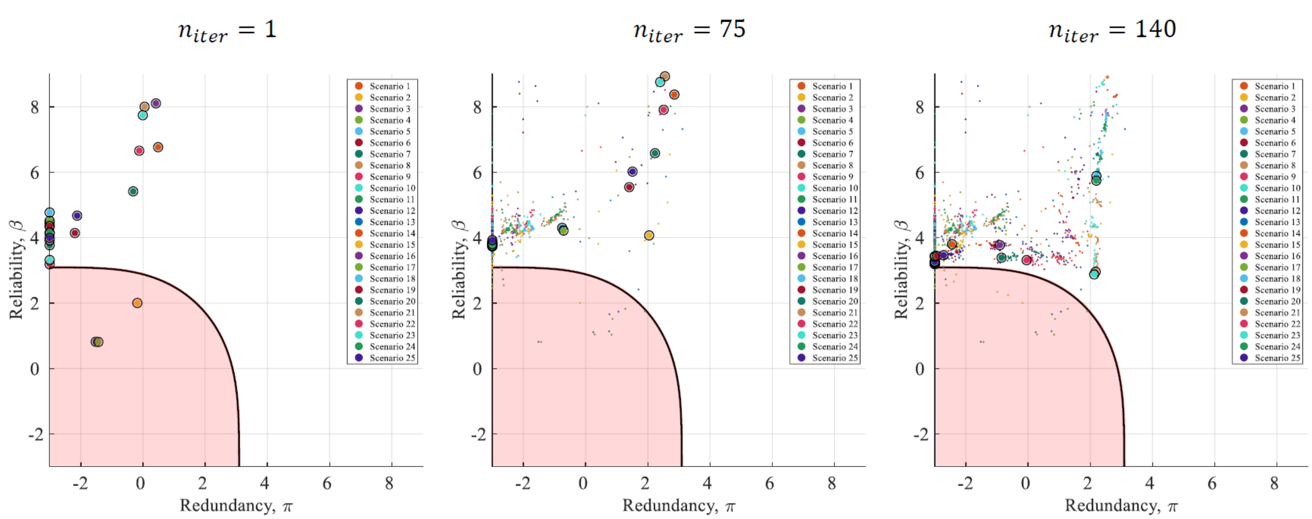

Figure 13: R3-DO process visualized by β-π diagrams at iteration steps #1, #75, and #140

6. CONCLUSIONS

This paper reviewed the system reliability-based disaster resilience analysis (S-DRA) framework recently proposed to address the pressing needs for probabilistic, multi-aspect, system-focused, and decision-making-oriented evaluation and management of disaster resilience of civil infrastructure systems. The β-π analysis method and diagram were successfully applied to real-world complex systems such as a cable-stayed bridge subjected to tank truck fire using sophisticated reliability methods. In applications to infrastructure networks under seismic hazards, causality-based component importance measures were developed based on the S-DRA framework. To promote various efforts toward risk intelligence of civil infrastructure systems, an optimization algorithm based on the S-DRA framework was also proposed and successfully demonstrated through its application to the design optimization of a truss bridge system. The framework enables us to understand disaster resilience in its multiple aspects: reliability, redundancy, and recoverability, and quantifies each criterion by state-of-the-art reliability analyses. Moreover, the β-π diagram provides insights into each aspect and their interrelationship to provide a holistic understanding of disaster resilience in the context of societal risks. Further research is needed to (1) extend its applications to another scale, such as urban communities, (2) understand the interrelationship between recoverability and the other two criteria, (3) deal with complexity in various real-world applications, and (4) streamline or automate optimal resilience-informed decision-making processes.

7. ACKNOWLEDGMENTS

The author sincerely thanks Mr. Seonghyun Lim, Mr. Youngjun Kwon (Seoul National University), Prof. Taeyong Kim (Ajou University), Dr. Sangri Yi, Dr. Jungho Kim (UC Berkeley), and Prof. Hyunjoong Kim (Liberty University) for their valuable contributions to the research presented in this paper.

8. REFERENCES

American Society of Mechanical Engineers (ASME). (2009). Innovative Technological Institute (ITI). Washington, D.C. ASME ITI, LLC.

Boore, D.M., and Atkinson, G.M. (2008). “Ground-motion prediction equations for the average horizontal component of PGA, PGV, and 5%-damped PSA at spectral periods between 0.01s and 10.0s.” *Earthquake Spectra*, 24(1), 99-138.

Bruneau, M., Chang, S.E., Eguchi, R.T., Lee, G.C., O’Rourke, T.D., Reinhorn, A.M., Shinozuka, M., Tierney, K., Wallace, W.A., and von Winterfeldt, D. (2003). “A Framework to quantitatively assess and enhance the seismic resilience of communities.” *Earthquake Spectra*. 19 (4): 733-752.

Chang, S.E., and Shinozuka, M. (2004). “Measuring improvements in the disaster resilience of communities.” *Earthquake Spectra*. 20 (3): 739-755.

Der Kiureghian, A. (2022). *Structural and System Reliability*, Cambridge University Press, New York, NY.

Echard, B., Gayton, N., and Lemaire, M. (2011). “AK-MCS: An active learning reliability method combining Kriging and Monte Carlo Simulation.” *Structural Safety*. 33: 145-154.

Ellingwood, B.R. (2006). “Mitigating risk from abnormal loads and progressive collapse.” *Journal of Performance of Constructed Facilities*. 20 (4): 315-323.

Hashimoto, T., Loucks, D.P., and Stedinger, J.R. (1982). “Reliability, resiliency, and vulnerability criteria for water resource system performance evaluation.” *Water Resources Research*. 18 (1): 14-20.

Hollings, C.S. (1973). “Resilience and stability of ecological systems.” *Annual Review of Ecology and Systematics*. 4: 1-23.

Hosseini, S., Barker, K., and Ramirez-Marquez, J.E. (2016). “A review of definitions and measures of system resilience.” *Reliability Engineering System Safety*. 145: 47-61.

Kang, W.-H., and Song, J. (2010). “Evaluation of multivariate normal integrals for general systems by sequential compounding.” *Structural Safety*. 32: 35-41.

Kwon, Y., and Song, J. (2023). “Decision-support measure for resilient infrastructure networks considering operation mechanism and cascading failure." *Proc. 14th International Conference on Application of Statistics and Probability in Civil Engineering (ICASP14)*, Jul 9-13, Dublin, Ireland.

Lee, J., Choi, K., Yoon, J., and Chung, C.-H. (2022). "Numerical analysis-based structural behavior assessment of a cable-stayed bridge under tanker fire." *Structure and Infrastructure Engineering*. 1-18.

Lim, H.W., and Song, J. (2012). "Efficient risk assessment of lifeline networks under spatially correlated ground motions using selective recursive decomposition algorithm." *Earthquake Engineering & Structural Dynamics*. 41(13): 1861-1882.

Lim, S., Kim, T., and Song, J. (2022a). "System-reliability-based disaster resilience analysis: Framework and applications to structural systems." *Structural Safety*. 96: 102202.

Lim, S., Kim., J., and Song, J. (2023). "Development of reliability-redundancy-recoverability-based decision optimization (R3-DO) for disaster resilience of structural systems." *Proc. 14th International Conference on Application of Statistics and Probability in Civil Engineering (ICASP14)*, Jul 9-13, Dublin, Ireland.

Lim, S., Yi, S., Kim, H.-J., and Song, J. (2022b). "Fire resilience evaluation of cable-stayed bridges through reliability-redundancy analysis." *Proc. International Conference on Structural Safety & Reliability (ICOSSAR 2021-2022)*, Sep 13-17, Shanghai, China.

Nielson, B.G., and DesRoches, R. (2007). "Analytical seismic fragility curves for typical bridges in the central and southeastern United States." *Earthquake Spectra*. 23(3): 615-633.

Pate-Cornell, E. (1994). "Quantitative safety goals for risk management of industrial facilities." *Structural Safety*. 13(3): 145–157.

Shokri, M., and Beyler, C.L. (1989). "Radiation from large pool fires." *Journal of Fire Protection Engineering*. 1(4): 141-150.

Tierny, K., and Bruneau, M. (2007). "Conceptualizing and measuring resilience: a key to disaster loss reduction." *TR News*, May-June, 250. 14-17.

Zhou, H., Wang, J., Wan., J., and Jia, H. (2010). "Resilience to natural hazards: a geographic perspective." *Natural Hazards*. 53: 21-41.